# Microstructure control and extrudability of aluminium-Mg-Si alloys microalloyed with manganese

S. Zajac, B. Hutchinson, A. Johansson, L.-O. Gullman, R. Lagneborg

JOURNAL DE PHYSIQUE IV
Colloque C7, supplément au Journal de Physique III, Volume 3, novembre 1993


# Microstructure control and extrudability of aluminium-Mg-Si alloys microalloyed with manganese

S. ZAJAC, B. HUTCHINSON, A. JOHANSSON*, L.-O. GULLMAN* and R. LAGNEBORG

*Swedish Institute for Metal Research, Drottning Kristinas Väg 48, 11428, Stockholm, Sweden*
** Gränges Technology Centre, 612 81 Finspång, Sweden*

*The hot deformation behaviour of AA 6063 and AA 6005 aluminium alloys has been related to chemical composition and the microstructural evolution occurring during the various heat treatment procedures prior to extrusion. It was shown that a small addition of manganese significantly accelerates the homogenising process (transformation of the plate-like beta-AlFeSi phase to the more rounded alpha-AlFeSi phase) which gives better hot formability and ductility. The mechanical behaviour of Al-Mg-Si alloys during hot working at low and intermediate strains was described by a new model for the accumulation and annihilation by climb of geometrically necessary dislocations at non-deformable precipitates. Strain hardening behaviour at high strains correlated with the reduction in spacing between grain boundary precipitates.*

## 1. INTRODUCTION

Aluminium alloys containing Mg and Si with small amounts of Fe as an impurity are widely used in extruded products because of their good extrudability and strength after age hardening. Prior to extrusion it is normal practice to give the cast billets a so called homogenisation heat treatment which serves two purposes. On the one hand it evens out micro-segregation of the fast diffusing species Mg and Si so ensuring solution of coarse $Mg_2Si$ precipitates. On the other hand it modifies the structure of the AlFeSi particles which are an insoluble phase in these alloys. Previous work (1, 2) has demonstrated convincingly that extrudability under industrial conditions depends strongly on the size and shape of the AlFeSi second phase particles. The present paper summarises some effects of alloy chemistry and heat treatment on microstructure and high temperature flow behaviour, and seeks to provide an explanation of the observed behaviour.

## 2. EXPERIMENTAL PROCEDURE

The materials in this investigation were commercially produced billets of alloys AA6063 and AA6005, details of which are summarised in Table 1.

**Table 1** Materials in this investigation.

| Alloy | Billet diameter | Mg | Si | Fe | Mn | Grain size |
|---|---|---|---|---|---|---|
| 6063-1 | ϕ 155 mm | 0.48 | 0.45 | 0.18 | 0.002 | 118 µm |
| 6063-2 | ϕ 155 mm | 0.49 | 0.41 | 0.15 | 0.049 | 97 µm |
| 6005-4 | ϕ 203 mm | 0.52 | 0.82 | 0.18 | <0.010 | 105 µm |
| 6005-5 | ϕ 203 mm | 0.53 | 0.77 | 0.19 | 0.041 | 101 µm |
| 6005-6 | ϕ 203 mm | 0.53 | 0.80 | 0.20 | 0.082 | 99 µm |

Small samples cut from these billets were homogenised between 545°C and 600°C for periods of 1 to 20 hours. Optical and scanning electron microscopy were used to characterise the microstructures. The AlFeSi particles were analysed quantitatively with respect to number, size and shape using an IBAS 2000 image analysis system. High temperature mechanical properties were measured in compression using specimens $\phi$10x15 mm. Specimens were heated at 3°C/s to the deformation temperature in the range 500°C to 600°C, then held at temperature for 6 minutes before straining at a nominal strain rate of 10/s.

## 3. RESULTS

Figure 1 demonstrates the types of second phase distribution which were observed in different samples depending on alloy chemistry and heat treatment. The AlFeSi particles lay mainly in grain boundaries where they had precipitated as platelets. With increasing homogenisation temperature and time these platelets broke up into necklaces of smaller spheroidised particles. Closer examination showed that the platelets were normally the monoclinic $\beta$-$Al_5FeSi$ phase which underwent an *in-situ* transformation to the cubic $\alpha$-$Al_{15}(FeMn)_3Si_2$ in association with the spheroidisation process.

Measurements of average particle shape factor after homogenisation anneals at 585°C are shown in Fig. 2 for both alloys. It is seen that particles in the AA6063 alloy spheroidise more readily as a result of the lower Si content than in AA6005 which tends to stabilise the $\beta$-$Al_5FeSi$ modification. The same effect is achieved by micro-alloying with Mn which is especially effective in accelerating the microstructural changes in AA6005 which otherwise are very sluggish.
True stress-true strain curves for the three AA6005 alloys at 500°C are shown in Fig. 3. Microstructures of these specimens were quite similar to those in Fig. 1. Initial yielding occurs at about the same stress in each case but the initial work hardening rates and subsequent flow stresses differ, being lower in the materials with well spheroidised second phases. Alloy 4 which contained the most elongated particles also showed prominent work hardening at high strain levels aboye $\varepsilon \sim 0.4$.

## 4. DISCUSSION

The present results demonstrate rather conclusively that it is the size and form of the second phases in these alloys which controls their high temperature plastic behaviour and accordingly their extrudability (1). Spheroidisation of these AlFeSi particles is enhanced by reduced silicon levels (as in AA6063) and by microalloying with manganese, both of which favour stability of the cubic $\alpha$-phase over the plate-like $\beta$-variant. Indeed, the beneficial effect of homeopathic additions of Mn in alloys of the AA6005 type is the most important practical consequence of the present work.

The role of second phase in general in controlling flow behaviour at both low and elevated temperatures is well recognised (eg 3, 4). An analysis by Humphreys and Kalu (5) suggests that there will be a critical size above which particles will dominate work hardening and microstructure development during straining at high temperatures. Their treatment predicts that for a given temperature (T) and strain rate ($\dot{\varepsilon}$), complete annihilation of dislocations by climb can occur for particles smaller than a critical size, $d_c$, whereas accumulation of dislocations will take place at larger particles. The analysis which is based on the climb rate of a single dislocation loop leads to a condition of the following type

$$d_c = \left(\frac{K \cdot D_v}{T\dot{\varepsilon}}\right)^{1/3} \qquad (1)$$

where $D_V$ = volume diffusion coefficient and K is a constant. Although this treatment is appealing in many ways and gives a temperature dependence in agreement with observation, the value of $KD_V$ deduced theoretically differs by several orders of magnitude from experimental values.

A new analysis has recently been developed by some of the present authors (6) based on the model shown in Fig. 4 where the climb rate of dislocation loops around a particle is accelerated by the accumulated stress fields of all the piled up dislocations. The treatment leads to a value of the climb velocity of a dislocation at position y' as

$$v_{climb} = \frac{2D_v Gb^3}{\pi(1-\nu)kT} \cdot \frac{ny'}{L^2} \qquad (2)$$

where G = shear modulus, b = magnitude of the Burger's vector, L = particle length, n = number of dislocation loops in the array.

The significant implications of the new treatment (6) are that the loops will always tend to be uniformly spaced (statistically) and that a steady state loop density will be approached corresponding to a steady state flow stress. Only extremely small particles (L < 0.04 μm for the present alloys and testing conditions) are expected to be free from dislocation loops. The flow stress contribution attributable to the particles at steady state is given by

$$\sigma_{ss} = \alpha G\left[\frac{6.2\pi(1-\nu)kT\dot{\varepsilon}}{D_v G}\right]^{1/4} \cdot L^{3/4}[(2r+L)p]^{1/2} \qquad (3)$$

where $\alpha$ = constant ≈ 1.5, 2r = particle thickness, p = number of particles/unit volume

Figure 5 shows experimental data for the AA6005 alloys plotted against the computed steady state strain hardening. A reasonable linear behaviour is observed which also extrapolates back to a yield stress of ~21 MPa, a value close to the measured yield stress of ~23 MPa. The different estimates of hardening differ by a factor of ~2.5 which is not unreasonable in view of various numerical uncertainties in the input data. Thus, it seems fair to conclude that hardening due to geometrically necessary dislocations around non-deformable particles accounts for the observed strain hardening in the present experiments.

According to the review of results assembled by Humphreys and Kalu (5) the critical particle size for the on-set of dislocation accumulation, $d_c$, should be ~6μm. The present treatment indicates that such a particle would be surrounded by some 2000 loops under steady state conditions which implies a different mechanism to that considered in the previous analysis (5).

In order to account for the extraordinary strain hardening behaviour at high strains two strengthening mechanisms were analysed. The first was fiber strengthening in which the AlFeSi particles should serve as a load bearing component. However, additional experiments on alloy 4 with oriented AlFeSi particles (0°, 45° and 90° after predeformation to $\varepsilon = 0.5$) gave similar values of the flow stress for all specimens which casts doubts over the relevance of fibre loading.

The second proposal follows the explanation by Embury and Fisher (7) for the accelerating strain hardening of pearlitic steels. Observations indicate that a cellular dislocation substructure is developed at the large AlFeSi particles during compression and the mean distance between substructural barriers, such as the grain boundary precipitates, decreases continuously with increasing strain. This produces a strain hardening that increases exponentially with strain. Following the approach used by Embury and Fisher (7) the flow stress, $\sigma_f$, above ~0.4 strain (after steady state condition) may be written in the form

$$\sigma_f = \sigma_i + \frac{k}{\sqrt{cd_i}}\exp(\varepsilon/2) \qquad (4)$$

where $\sigma_i$ = flow stress at $\varepsilon$ ~0.4, k is equivalent to the Petch slope, $d_i$ = mean distance between the grain boundary precipitates and c = geometrical factor ~2

The results obtained from compression tests and eqn. (4) are plotted in Fig. 6. The predicted relationship is seen to be obeyed in all cases but with a higher slope in the case of alloy 6005-4. When the intergranular coverage of precipitates is high, as in alloy 6005-4 ,Fig 1a, this mechanism operates effectively, whereas its effect diminishes when the coverage of grain boundary particles decreases, as in Fig. 1b.

## 5. REFERENCES


1. L-O. Gullman, S. Zajac and A. Johansson, 5th Int. Alum. Ext. Tech. Sem., Chicago, 1992, vol. 2, 71-77.
2. S. Zajac, L-O. Gullman and A. Johansson, 3rd Int. Conf. on Aluminium Alloys, Trondheim, 1992, vol. 2, 133-139.
3. M.F. Ashby, Strengthening Methods in Crystals, John Wiley & Sons, New York, 1971, p. 137.
4. L.M. Brown, Proc. 3rd Risö Int. Symp., Ed. E. Lillholt, 1982, pp. 1-18.
5. F.J. Humphreys and P.N. Kalu, Acta Met., 1987, 35, 2815.
6. R. Lagneborg, S. Zajac and W.B. Hutchinson ,Scripta Met. et Mat., 1993, vol. 29, 6.
7. J.D. Embury and R. M. Fisher, Acta Met., 1966, 14, 147.

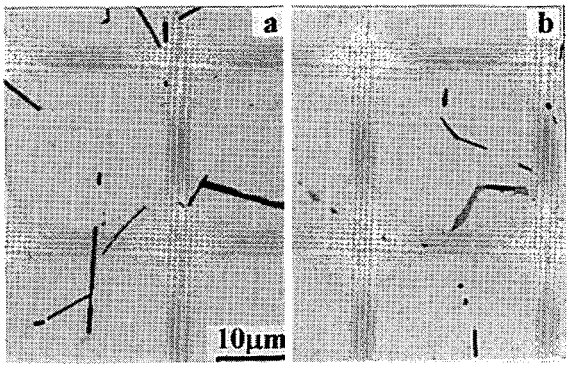


Fig. 1 Microstructure of AA 6005-4 (a) and -5 (b) after homogenisation at 585°C for 2 hours.

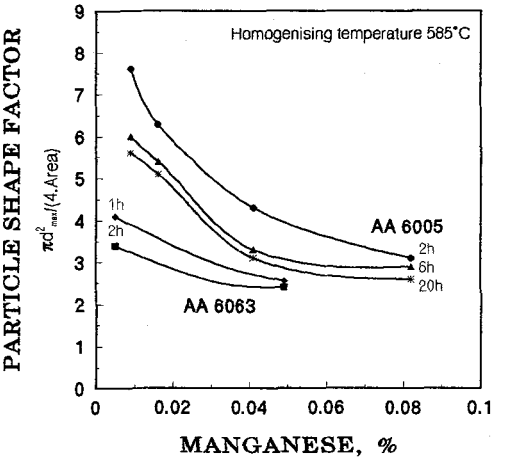


Fig. 2 Average particle shape factor in AA 6063 and AA 6005 after homogenisation at 585°C as a function of Mn contents.

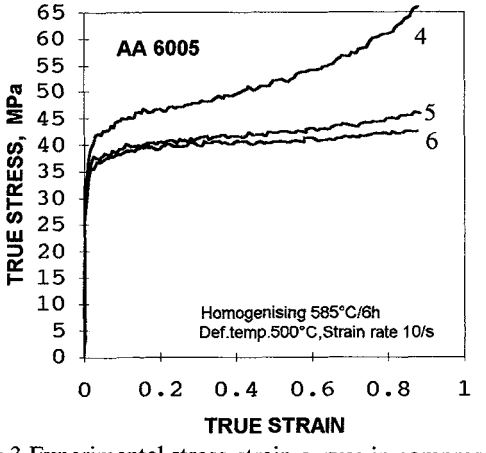


Fig.3 Experimental stress-strain curves in compression for Mn-modified AA 6005; 4 without Mn, 5 with 0.041%Mn and 6 with 0.082%Mn.

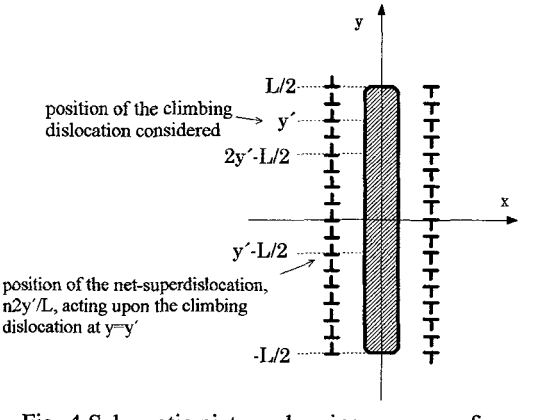


Fig. 4 Schematic picture showing an array of n dislocation loops captured during straining around a plate-like particle.

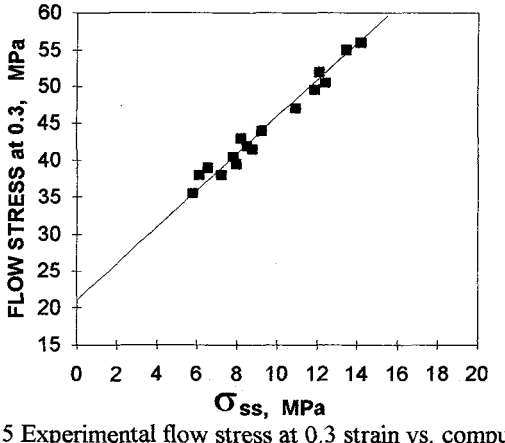


Fig. 5 Experimental flow stress at 0.3 strain vs. computed steady state strain hardening, $\sigma_{ss}$, from Eq. (3) for $\alpha = 1.55$ (6), G = 26 GPa and $D_V = 6.7 \cdot 10^{-10}$ cm²/sec.

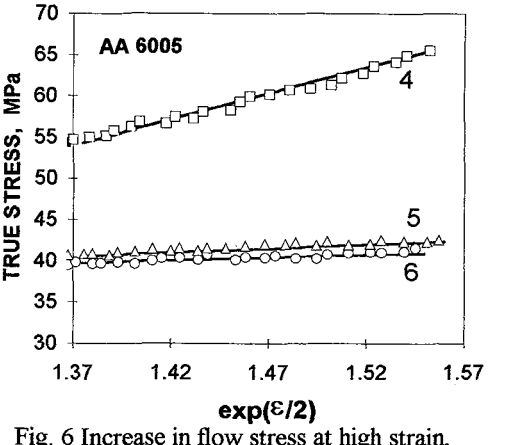


Fig. 6 Increase in flow stress at high strain, plotted according to equation (4) in text.